International Journal of Digital Earth

ISSN: 1753-8947 (Print) 1753-8955 (Online) Journal homepage: www.tandfonline.com/journals/tjde20

Atacama Field Campaign: laboratory and in-situ measurements for remote sensing applications

Cristian Mattar, Andrés Santamaría-Artigas, Flavio Ponzoni, Cibele T. Pinto, Carolina Barrientos & Glynn Hulley

To cite this article: Cristian Mattar, Andrés Santamaría-Artigas, Flavio Ponzoni, Cibele T. Pinto, Carolina Barrientos & Glynn Hulley (2019) Atacama Field Campaign: laboratory and in-situ measurements for remote sensing applications, International Journal of Digital Earth, 12:1, 43-61, DOI: 10.1080/17538947.2018.1450901

To link to this article: https://doi.org/10.1080/17538947.2018.1450901

INTERNATIONAL JOURNAL OF DIGITAL EARTH
2019, VOL. 12, NO. 1, 43–61
https://doi.org/10.1080/17538947.2018.1450901

Atacama Field Campaign: laboratory and in-situ measurements for remote sensing applications

Cristian Mattar[a], Andrés Santamaría-Artigas[b], Flavio Ponzoni[c], Cibele T. Pinto [c], Carolina Barrientos[d] and Glynn Hulley[e]

[a]Laboratory for Analysis of the Biosphere (LAB), University of Chile, Santiago, Chile; [b]Department of Geographical Sciences, University of Maryland, College Park, MD, USA; [c]Divisão de Sensoriamento Remoto (DSR), Instituto Nacional de Pesquisas Espaciais (INPE), São Paulo, Brasil; [d]Aerial Photogrammetric Service (SAF), Chilean Air Force, Santiago, Chile; [e]Jet Propulsion Laboratory (JPL), California Institute of Technology, Pasadena, CA, USA

ABSTRACT

This work presents the preliminary results of the first field calibration campaign performed in the Atacama Desert, Chile, between the 18 and 22 August 2014, called the Atacama Field Campaign (ATAFIC 2014). In situ measurements were performed in order to spectrally characterize the surface reflectance spectra between 0.3 and 2.5 µm, radiometric temperature (8.0–14.0 µm) and atmospheric measurements. A soil sample was collected and analyzed using Fourier Transform Infrared Spectroscopy and X-Ray Diffraction techniques to characterize the surface reflectance spectra and mineralogical composition, respectively. ASTER land surface emissivity in addition to GOES, MODIS and Landsat-8 land surface temperature (LST) were also used. Results showed that the spectral features of the Atacama soil and the characteristics of this geographical zone, which is featured as the most hyper-arid and cloudless place in the world, make this area a potential target for surface reflectance characterization. Day and night LST comparison between field and remote sensing data are lower than 2 K and the Root Mean Square Error for land surface emissivity is close to 2%. This work opens the possibilities to consider the Atacama Desert as a reference target for calibration and validation activities for earth observation missions' purposes.

ARTICLE HISTORY
Received 2 August 2017
Accepted 7 March 2018

KEYWORDS
Atacama; spectroradiometry; emissivity; temperature; surface reflectance

1. Introduction

The choice of suitable and representative areas for vicarious calibration campaigns is a requirement that helps in the success of any earth observation (EO) mission and its retrievals. Several land cover types have been used as test sites for different EO missions, not only for the calibration and validation of the radiometric features of on-board sensors, but also for the products developed from remote sensing data. For instance, agricultural mixed areas (Sobrino et al. 2008, 2011; Krishnan et al. 2015), barren surfaces such as deserts, lunar or polar zones (Chander et al. 2013), pastures, crops, grasslands and mixed natural landscapes, among others (Franch, Vermote, and Claverie 2014).

Both identification and monitoring of representative targets contribute to ensure the traceability of on-board instruments and also to assess the uncertainty of its measurements in order to be useful for detecting long-term trends (Chander et al. 2013). These targets must be selected considering surface characteristics such as spectral behavior (in terms of high surface reflectance), spatial

CONTACT Cristian Mattar cmattar@uchile.cl

representativeness, temporal stability and atmospheric conditions such as low aerosol loading, low water vapor content and high frequency of clear-sky days, among other criteria (Scott, Thome, and Brownlee 1996). In this context, the Committee on Earth Observation Satellites (CEOS) (http://ceos.org) has recommended a set of well-characterized sites across the world, which are instrumented with ground sensors for a detailed monitoring of surface and atmospheric conditions (Chander et al. 2013). These sites are mainly classified into two different groups: Well-instrumented and pseudo-invariant calibration sites (PICS). The well-instrumented sites are used for field campaigns with the aim of obtaining absolute radiometric parameters, facilitating the traceability and inter-comparison to evaluate the biases of future and in-flight instruments in a consistent manner. Meanwhile, PICS are focused on the evaluation of the long-term stability of instruments on-board satellites and the inter-comparison of multiple instruments. PICS correspond to desert areas with sand dunes, low aerosol loading, high surface reflectance and no vegetation. These sites have been widely used for absolute radiometric cross calibrations, to evaluate the long-term stability of on-board satellite instruments and also for inter-comparison of multiple sensors (Helder et al. 2013; Lacherade et al. 2013). A representative example of the applicability of both kinds of sites is presented by Campbell et al. (2013) that focuses on the comprehensive calibration and validation process of EO-1 Hyperion over PICS and well-instrumented flux sites.

The high scientific interest in deserts can be seen by the results of previous research where these areas have been demonstrated to be good candidates for the assessment of multi-temporal, multi-band or multi-angular calibration of optical satellite sensors (Cosnefroy, Leroy, and Briottet 1996; Nagaraja Rao et al. 1999; Miesch et al. 2003; Govaerts and Clerici 2004; Olesen and Göttsche 2009; Bullard, White, and Livingstone 2011; Hulley, Hook, and Baldridge 2009; Göttsche and Hulley 2012; Jiménez-Muñoz et al. 2013). Despite the advantages of desert zones, one of the most relevant desert in the world, the Atacama Desert, has only recently began to be used for exploratory remote sensing field campaigns.

The Atacama Desert is located in the west side of the Andes Mountains and covers the southern part of Peru, the western part of Bolivia and the Northern part of Chile. Different ecosystems, landscapes and biomes are present in these zones (Moreira-Munoz 2011). The hyper-arid conditions that characterize the Chilean part of the Atacama Desert have been targeted by several works in different scientific areas such as: geochemistry, soils and biology, astrobiology, lunar vehicles, mars analog, mineral mapping (Wettergreen et al. 1999; Richards, Boyce, and Pringle 2001; Brown, Wild, and Cunningham 2004; Hubbard and Crowley 2005; Clarke 2006; Lester, Satomi, and Ponce 2007; Muñoz et al. 2007; Ramachandran, Justice, and Abrams 2011; Azua-Bustos, Urrejola, and Vicuña 2012; Fletcher et al. 2012; Morgan et al. 2014; Wang et al. 2014) and most recently the assessment of Tamarugo (*Prosopis tamarugo*), which is the only forest in the world that grows under hyper-arid conditions (Chávez et al. 2012, 2013). Besides these scientific approaches, one of the most important and highlighted interests in the Chilean part of the Atacama Desert is related to astronomy applications. The Atacama Desert gathers two of the most important telescopes and radio astronomy experiments in the world: The Atacama Large Millimeter Array (ALMA) (Brown, Wild, and Cunningham 2004), located in Chajnantor plateau and the European Extremely Large Telescope, installed in Cerro Armazones, making the Atacama Desert one of the most important space observation places in the world. Above all, its low atmospheric water vapor content, high altitude and frequency of cloudless days were the main features that led the selection of the Atacama Desert for the establishment of astronomical projects; and also make it suitable for remote sensing purposes. However, the Atacama Desert has never been considered as a possible site to become a target standard zone for remote sensing calibration or validation purposes. Previous experiments have described the atmospheric characterization of the Atacama desert (Pinto et al. 2015; Cordero et al. 2016), although the characterization of a target area in the Atacama Desert with remote sensing, in-situ and laboratory measurements have not been conducted yet for remote sensing calibration or validation activities. A well site characterization can be used for further definition of a well representative site in the Atacama desert. Thus, the objective of this manuscript is to present the first remote

sensing field campaign carried out in the Atacama Desert describing laboratory (FT-IR, XRD and chemical analysis) and in-situ measurements (surface reflectance spectra, radiometric temperature and soil moisture). The structure of this paper is detailed as follows: Section 2 shows the study area and data acquisition protocol, Section 3 shows the obtained results, the discussion is presented in Section 4, and the conclusions about this work are shown in Section 5.

2. Study area

The Atacama Desert is the most arid zone in South-America and probably in the Earth. This area is characterized by a west–east altitudinal gradient and desert climate types (Cereceda et al. 2008). Its aridity can be attributed to the interactions between the large-scale atmospheric circulation, Humboldt current along the coast and the Andes mountain range, generating a low mean annual precipitation in the central depression, coastal fog and seasonal rainfall events in the high elevations of the Andes mountain range (Rodwell and Hoskins 2001; Takahashi and Battisti 2007; Cereceda et al. 2008; Garreaud, Molina, and Farias 2010; Insel, Poulsen, and Ehlers 2010). In terms of paleoclimate, the Atacama Desert changed from arid to hyper-arid conditions generating its current features (Rutllant, Fuenzalida, and Aceituno 2003; Clarke 2006), although there is still no clear consensus about the reasons of this extreme condition as detailed and described by Garreaud, Molina, and Farias (2010). Despite the widespread sites to be found in the Atacama Desert for remote sensing application or field campaigns, we have focused our efforts in an area close to the San Pedro de Atacama town, named 'El Tambillo'. The 'El Tambillo' area is located at 2438 m above sea level (m.a.s.l), 22 km south-west from San Pedro de Atacama town and close to the ALMA-Operations Support Facility. The area belongs to an alluvial fan (i.e. alluvial deposit) composed of gravel, sand and silt, originated during Pleistocene-Holocene (Servicio Nacional de Geología y Minería de Chile (Sernageomin) 2003). 'El Tambillo' was chosen because of the flatness and homogeneity of the surface, its atmospheric conditions (e.g. low aerosol loading and clear sky), the suitability to be monitored by several optical sensors with different spatial resolution (0.50–5000 m^2), and its accessibility (i.e. short distance from the main road).

3. Data acquisition

3.1. In situ measurements

Surface reflectance, radiometric temperature and direct solar irradiance in-situ measurements were conducted over 'El Tambillo'. In this area, a hyperspectral surface reflectance characterization was made in the 0.35–2.5 μm region using a FieldSpec®- 4 spectroradiometer (Analytical Spectral Devices®, ASD). Additionally, a parallel characterization of spectral behavior ranged from 0.4 to 1.0 μm was conducted using a FieldSpec® HandHeld (ASD) spectroradiometer. White reference measurements were obtained from two Spectralon® (0.3 and 0.1 m^2) standard reference panels (one per instrument). Land leaving radiance measurements in the TIR domain (8.0–14.0 μm) were computed from brightness temperature (BT) measurements performed automatically every 10 s using an SI-111 (Apogee®) thermal radiometer was first mounted on a tripod 1 m above ground at a 30 degree angle for an approximate footprint of 0.86 m^2, and later mounted on a vehicle at 1.5 m also at 30 degree angle for an approximate footprint of 1.93 m^2. Thermal downwelling irradiance was estimated by measuring sky BT, targeting at the sky in the opposite direction of the sun. Aerosol optical depth and atmospheric water content were computed from direct solar irradiance measurements performed with a portable CIMEL CE-317 (CIMEL Electronique®), mounted on a tripod and pointing at the sun during the whole measurement period. Solar radiation was measured at five channels (i.e. 0.440, 0.670, 0.870, 0.936 and 1.020 μm central wavelengths) with a 1.2° FOV. Finally, one soil sample from the study area was collected for further laboratory analysis. Table 1 summarizes the in-situ measurements carried out during ATAFIC 2014.

Table 1. Instruments, measuring protocol and magnitude retrieved between 19 and 22 August 2014.

Instruments	Measurement protocol	Measure	Units
CIMEL CE – 317	Mounted on a tripod in order to provide continuous measurements during the field activities	Solar irradiance	W m^{-2}
ASD FieldSpec – 4	Transects in 300 m^2 grid	Surface reflectance (0.35–2.5 μm)	%
ASD FieldSpec HandHeld	- Transects in 100 m^2 grid - 2 km transects in vehicle	Surface reflectance (0.4–1 μm)	%
Apogee SI111	- Mounted on a tripod in order to provide continuous measurements during the field activities - 2 km transects in vehicle	Brightness temperature (8.0–14.0 μm)	K

The ASD FieldSpec-4 was used to measure the surface reflectance over an area of 300 m^2. In this area, the same protocol for measuring surface reflectance was applied daily during ATAFIC at the same local time, in order to account for temporal variations of the surface reflectance. More details of this surface and the hyperspectral characterization in addition to the atmospheric composition in terms of water vapor and aerosol loading can be found in Pinto et al. (2015).

A FieldSpec-HandHeld spectroradiometer and an Apogee SI-111 thermal radiometer were used for measuring the surface reflectance and BT over a different area of approximately 100 m^2. This integrated measurement protocol has been previously applied and published (Sobrino et al. 2012). The surface reflectance measurements were conducted over the 100 m^2 square area, while the BT was continuously measured at the center of the square. Moreover, based upon past experiences in which geostationary thermal data has been validated by using off-road vehicles (Göttsche, Olesen, and Bork-Unkelbach 2013), integrated SR and BT measurements were performed over a 2 km-long transect to characterize the spatial heterogeneity. Figure 1 shows the study area and the sampling method applied during ATAFIC.

Land Surface Temperature (LST) was computed from surface brightness temperature (TBsuf) using Equation (1) based on an approximation of the radiative transfer equation:

$$B(\mathrm{LST}) = \frac{\mathrm{Lrad} - (1-\varepsilon)\mathrm{Ldown}}{\varepsilon}, \tag{1}$$

where Lrad is the land leaving radiance (W m^{-2}) measured by a thermal radiometer, ε is the land surface emissivity, Ldown is the long-wave downwelling irradiance (W m^{-2}) converted from the TBsky measured by the thermal radiometer and B(LST) is the Planck's law for the LST (W $m^{-2}sr^{-1}\mu m^{-1}$). Finally, the LST (K) was estimated by inverting the Planck's law.

3.2. Laboratory measurements

The collected soil sample was analyzed in the laboratory to determine its emissivity spectra, mineralogical composition and texture. Previous work has demonstrated the potential use of soil characterization for remote sensing applications when FT-IR reflectance/emissivity spectra and XRD-diffraction analysis are combined (Sobrino et al. 2009). The emissivity spectrum of the collected soil sample was obtained from hemispherical reflectance measurements carried out at NASA's Jet Propulsion Laboratory in Pasadena, California (USA) and converted to emissivity using Kirchhoff's law. Measurements were performed using a Nicolet® 520 FT-IR spectrometer equipped with a Labsphere® integrating sphere. Other equipment characteristics and sample preparation protocols are detailed in Baldridge et al. (2009).

In order to determine the mineralogical soil composition, an X-Ray diffraction (XRD) analysis was also conducted. For this purpose, the soil sample was sieved using a 200-mesh grid, after that, it was pulverized in an agate mortar. Then, an X'Pert Pro diffractometer from PANalytical® was used to identify the possible minerals contained in the soil sample. Measurements of X-ray

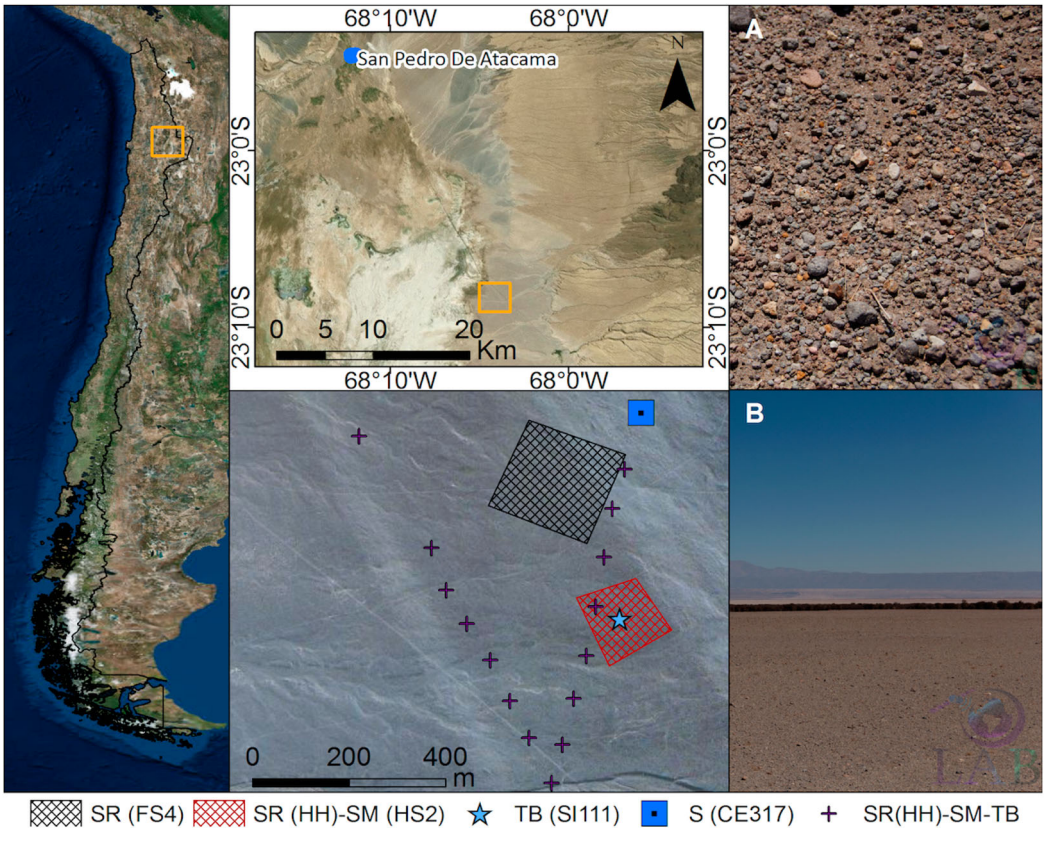

Figure 1. Study area and distribution of the surface reflectance (SR) (dashed areas) location of the solar irradiance (S) measurements (square), and location of the brightness temperature (BT) measurements and soil sample collection point (star). The crosses show the sampling points of the 2 km vehicle transect. Pictures: (A) Close-up of the study area surface showing pebbles, and (B) view of the 'Tamarugo' forest from the study area.

powder diffraction were collected at 2θ from 3° to 70°, with a step size of 0.02°. The copper anode X-ray source was operated at 40 kV and 30 mA, giving a count rate of 2 s/step. Finally, the texture, electrical conductivity, anions, cations and salinity were obtained by chemical analysis.

4. Method

Different surface reflectance and emissivity values were derived for several spectral bands of the most used optical sensors such as the Advanced Spaceborne Thermal Emission and Reflection Radiometer (ASTER) on board the Terra Satellite, the Moderate Resolution Imaging Spectroradiometer (MODIS) on board the Terra and Aqua satellites, the Enhanced Thematic Mapper Plus (ETM+) on board Landsat 7, the Operational Land Imager (OLI) and Thermal Infrared Sensor (TIRS) on board Landsat 8, and the New AstroSat Optical Modular Instrument-1 (NAOMI-1) on board the Chilean satellite Fasat-Charlie. With this aim, the surface reflectance and emissivity spectra were convolved with the relative spectral response of each sensor band using the RSR calculator software (Durán-Alarcón et al. 2014). The convolved emissivities were then compared to values obtained from the ASTER Global Emissivity Dataset (GED) v3 (Hulley et al. 2015) for the study area. The emissivity values from the ASTER GED product are the result of averaging all ASTER observations in time from 2000 to 2008 into a single value, since each pixel's standard deviation is also included in the product it was possible to characterize the spatial and temporal variation of emissivity in the

study area by means of the coefficient of variation (CV) showed in Equation (2):

$$\mathrm{CV} = \frac{\mathrm{SDEV}}{\bar{x}}, \tag{2}$$

where SDEV and $\bar{x}$ are the standard deviation and mean of a single pixel through time, respectively.

LST at different spatial resolutions was obtained from Geostationary Operational Environmental Satellites (GOES) (~5000 m^2), MODIS (~1000 m^2) and L8 TIRS (~100 m^2). The GOES GEO-LAND-2 LST product uses a Dual-Algorithm proposed by Freitas et al. (2013). In the case of MODIS, the LST retrieval uses a generalized split-window algorithm over clear-sky conditions (Wan 1999). For this study, the MOD11A1 collection 5 product was used. Finally, LST from L8 TIRS data was estimated using the single channel algorithm proposed by Jiménez-Muñoz et al. (2014) and using the Global Atmospheric Profiles from Reanalysis Information database (Mattar et al. 2015). It is noteworthy that although the L8 TIRS data is originally acquired at a resolution of 100 m^2, the distributed product is delivered at 30 m^2 after a cubic convolution resampling in order to match the OLI multispectral bands.

5. Results

5.1. Surface characterization

The surface of the study area is mainly covered by sand and pebbles; then, it is thought it was originated by alluvial-fan formative processes (Jungers et al. 2013). According to the results of the XRD analysis, the mineralogical composition of the ATAFIC zone soil is mainly composed of labradorite ($(Ca,Na)(Al,Si)_4O_8$), quartz (SiO_4) and magnetite (Fe_3O_4). Other minerals such as microcline, intermediate muscovite (sericite), biotite, ferroactinolite and traces of montmorillonite were present in the sample. The mineral composition of the sample coincides with the chemical analysis (Table 2), that reveals the concentration of cations and anions. The texture of the site was identified as sandy loam.

The surface emissivity spectra obtained in the laboratory is shown in Figure 2. The sand sample has two different grain sizes, the fine grain representative of sand and the coarse grain that correspond to the pebbles. In terms of emissivity, sand and pebbles show a similar spectral behavior, although different magnitudes. Despite the fact that the emissivity spectra were obtained using an infragold integrating sphere that avoids bi-directional effects in the TIR (Salisbury, Wald, and D'Aria 1994), the fine-grained soil samples (i.e. sand) showed a slightly lower magnitude than mixed ones or coarse-grained samples (i.e. sand and pebbles, or only pebbles, respectively). A possible anisotropic effect added by the pebbles could explain this increase in the emissivity values or it

Table 2. Textural and chemical analysis of the Atacama soil sample.

Parameters	Units	Values
Sand (2–0.05 mm)	%	79.3
Silt (0.05–0.002 mm)	%	14.8
Clay (<0.002 mm)	%	5.9
Ca^{2+}	mmol+/L	7.77
Mg^{2+}		0.61
Na^{+}		1.90
K^{+}		0.56
SO_4^{2-}	mmol-/L	0.065
Cl^{-}		0.51
HCO^{3-}		0.01
pH	unitless	7.98
Electrical conductivity (EC)	dS/m	0.88
Sodium absorption ratio (SAR)	unitless	0.93
Percentage of interchangeable sodium (ESP)	%	1.36
Water saturation		21.01

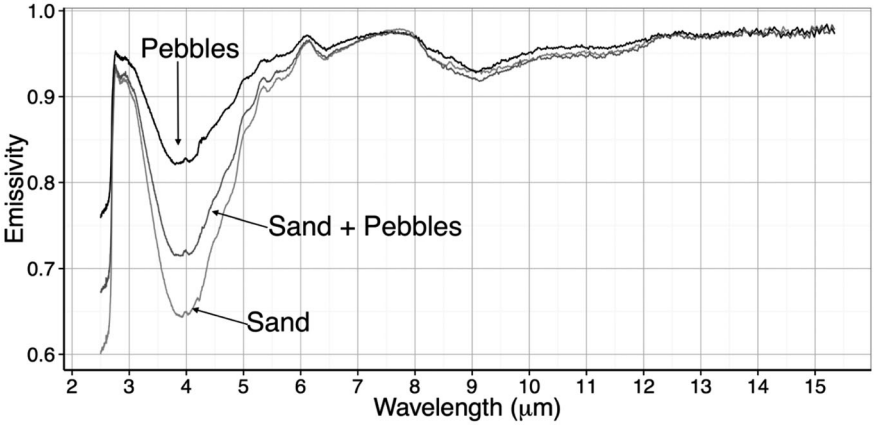

Figure 2. Soil emissivity spectra for the sand, pebbles and mixed sand and pebbles samples collected in the field.

could be attributed to the mineralogical differences since the sand probably has more clay content than pebbles (Salisbury and D'Aria 1992). The average difference between the pebbles and sand emissivities in the TIR window (8.0–14.0 μm) is approximately 2.1%.

The surface reflectance spectra measured with the ASD FieldSpec HandHeld (HH) and FieldSpec 4 (F4) are presented in Figure 3. Despite the surface reflectance spectra retrieved from HH is slightly higher in magnitude, both spectra are similar with a Root Mean Square Error (RMSE) equal to 0.8% between 0.4 and 1.0 μm and a coefficient of determination (r^2) equal to 0.998. The highest standard deviation values were obtained around 0.75 μm, while the minimum standard deviation was located in the region between 0.5 and 0.6 μm. The region close to 1.0 μm presents a possible background noise evidenced in the HH, as well the region close to 0.4 μm. This could probably be attributed to the sensitivity of the instrumentation in the limits of the bandwidth. The noise influences are

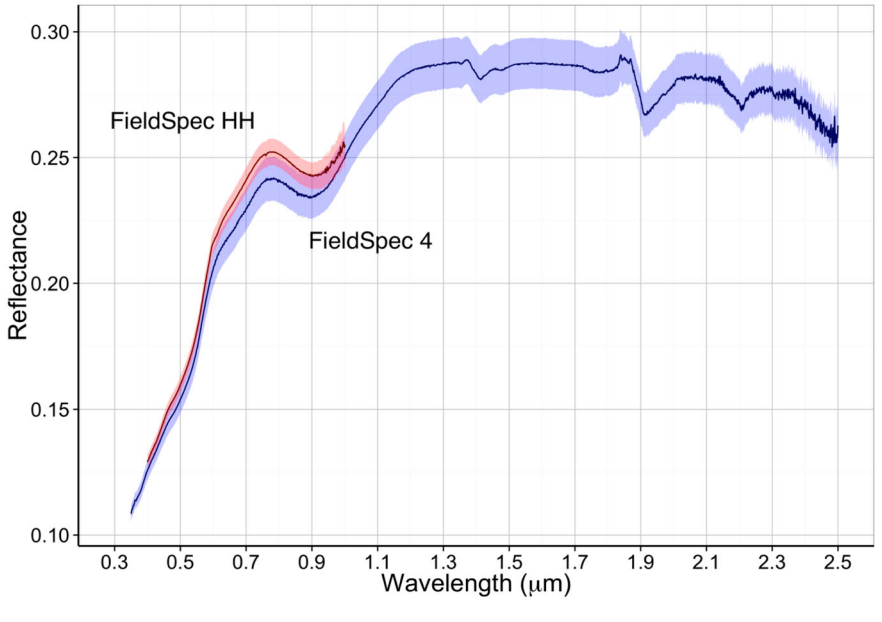

Figure 3. Mean surface reflectance for Atacama soil sample derived from FieldSpec HH (0.4–1.0 μm) and FieldSpec 4 (0.35–2.5 μm) on 19 August 2014. The standard deviations for FieldSpec HH and Fieldspec 4 measurements are also shown.

also evidenced in the spectral domain between 2.3 and 2.5 μm for the F4. As for the atmospheric parameters retrieved during the field campaign, the optical depth ranged between 0.04 and 0.362 for the 440 and 870 nm wavelengths, respectively, and the water vapor concentration was lower than 0.4 g cm^{-2}. A detailed analysis of the atmospheric characterization in addition to the surface spectra measured by FieldSpec4 appears in Pinto et al. (2015).

5.2. In-situ measurements and remote sensing comparison

Based on the GED data, the mean emissivity for each band shows low spatial variations in the study area and mostly in the site where the soil sample was acquired (Figure 4). Nevertheless, the CV (Equation 2) shows values of up to 0.3% for the bands located between 8.1 and 9.3 μm (bands 10, 11 and 12), in contrast to the bands located in the range between 10.2 to 11.7 μm (bands 13 and 14), where the CV is low (less than 0.09%). Despite this spatial variability, the area where the measurements were carried out, present a very low CV, ranging between 0.1% for band 10, and 0.01% for band 14. The highest CV was observed far from the area where the measurements were performed, specifically located near to the Atacama salt pan that presents high anisotropy structure and it is influenced by external parameters such as weather conditions (e.g. wind, temperature) and mining activities.

The importance of land surface emissivity and reflectance characterization of the study area in the Atacama Desert is highly related to the main applications in remote sensing for comparing in-situ measurements with satellite retrievals and also key for vicarious calibration processes. Thus, Table 3 shows the land surface reflectance convolved for the most commonly used remote sensors such as OLI (Landsat 8), ETM+ (Landsat 7), ASTER (Terra) and MODIS (Terra and Aqua). Additionally, values for the Chilean sensor NAOMI (Fasat-Charlie) are also shown. All these sensors are capable of monitoring the study area of ATAFIC, and the in-situ surface measurements can fulfill the requirements to validate or even calibrate the land surface products derived from the data provided by the mentioned sensors. Despite the fact that slight variations can be observed when comparing the surface reflectance retrieved by two different spectroradiometers, the magnitudes for each sensor band are quite similar and did not show any significant variation.

Table 4 shows the surface emissivity derived in the laboratory from the soil sample and convolved for each of the thermal band of the OLI, ETM+, ASTER and MODIS sensors. These values are a first approximation which could be considered in further evaluation the current and future thermal remote sensing missions. Figure 5 shows the comparison between the land surface emissivity from the lab measurements convolved to the five ASTER bands and the ASTER GED emissivity product.

These results show a slight bias (~3%) in the emissivity values for ASTER bands 10, 11 and 12 even though the spectral shapes match closely. However, for bands 13 and 14, the bias was lower (0.6%) showing a good performance between laboratory and GED data. The bias in bands 10–12 could be attributed to the ASTER emissivity calibration curve, which is derived from a subset of the ASTER spectral library, not accounting for the types of soils found in this region. The standard deviation of each ASTER band also evidenced the stability in the magnitude of the emissivity values, showing a higher amplitude at ASTER bands located between 8.1 and 9.3 μm when compared with the bands located in the 10.2 and 11.7 μm region. The RMSE for sand, pebbles and mixed samples (sand and pebbles), in average for all bands were 2.8, 3.2 and 2.5%, respectively, suggesting a good agreement between the laboratory and GED data, despite the possible bias located in some of the ASTER bands.

In terms of the spatial distribution, the emissivity values obtained from GED data did not show any significant variation in terms of CV values, because of typically constitute a spatially homogenous surface. These results represent a first comparison between laboratory and remote sensing data in order to demonstrate the possible applications of the study area for further remote sensing

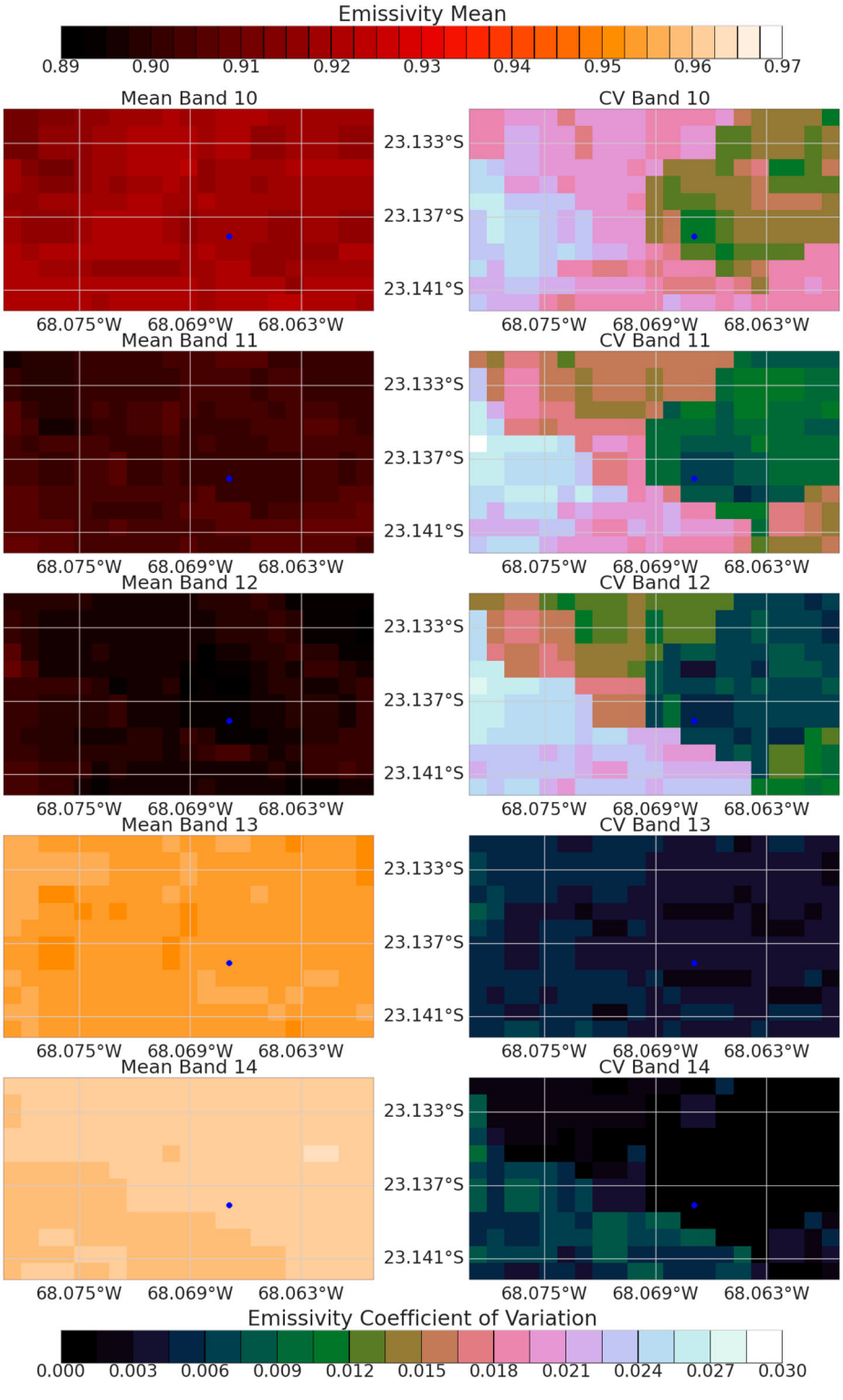

Figure 4. Mean emissivity (left) and emissivity's coefficient of variation (right) of the study area, for ASTER bands 10–14, obtained from the ASTER GED 100 m product. The blue dot shows the location where the soil sample was collected.

Table 3. Mean and standard deviation (σ) of surface reflectance values measured with ASD HandHeld (HH) and Fieldspec 4 (F4) filtered for different bands of several sensors.

Band (Bandwidth μm)	$\rho \pm \sigma$ (HH)	$\rho \pm \sigma$ (F4)	MODIS	$\rho \pm \sigma$ (HH)	$\rho \pm \sigma$ (F4)
OLI-01 (0.43–0.45)	0.143 ± 0.003	0.139 ± 0.005	B01 (0.62–0.67)	0.229 ± 0.005	0.218 ± 0.008
OLI-02 (0.45–0.51)	0.155 ± 0.003	0.150 ± 0.005	B02 (0.84–0.88)	0.246 ± 0.005	0.236 ± 0.009
OLI-03 (0.53–0.59)	0.190 ± 0.004	0.182 ± 0.006	B03 (0.46–0.47)	0.151 ± 0.003	0.145 ± 0.005
OLI-04 (0.64–0.67)	0.231 ± 0.005	0.220 ± 0.008	B04 (0.55–0.57)	0.184 ± 0.004	0.176 ± 0.006
OLI-05 (0.85–0.88)	0.245 ± 0.005	0.235 ± 0.009	B05 (1.23–1.25)	–	0.286 ± 0.010
OLI-06 (1.57–1.65)	–	0.288 ± 0.010	B06 (1.63–1.66)	–	0.287 ± 0.010
OLI-07 (2.11–2.29)	–	0.287 ± 0.010	B07 (2.11–2.16)	–	0.281 ± 0.010
OLI-08 (0.50–0.68)	0.204 ± 0.004	0.195 ± 0.007	B08 (0.41–0.42)	0.133 ± 0.003	0.129 ± 0.004
OLI-09 (1.36–1.38)	–	0.276 ± 0.010	B09 (0.44–0.45)	0.143 ± 0.003	0.139 ± 0.005
ETM+-01 (0.42–0.52)	0.154 ± 0.003	0.148 ± 0.005	B10 (0.48–0.49)	0.156 ± 0.003	0.150 ± 0.005
ETM+-02 (0.52–0.60)	0.190 ± 0.004	0.182 ± 0.006	B11 (0.53–0.54)	0.171 ± 0.003	0.164 ± 0.006
ETM+-03 (0.63–0.69)	0.232 ± 0.005	0.222 ± 0.008	B12 (0.55–0.56)	0.179 ± 0.004	0.172 ± 0.006
ETM+-04 (0.77–0.90)	0.248 ± 0.005	0.238 ± 0.009	B13 (0.66–0.67)	0.233 ± 0.005	0.222 ± 0.008
ETM+-05 (1.55–1.75)	–	0.287 ± 0.010	B14 (0.67–0.68)	0.236 ± 0.005	0.225 ± 0.008
ETM+-07 (2.09–2.35)	–	0.277 ± 0.010	B15 (0.74–0.75)	0.250 ± 0.005	0.239 ± 0.009
ETM+-08 (0.52–0.90)	0.233 ± 0.005	0.223 ± 0.008	B16 (0.86–0.88)	0.245 ± 0.005	0.235 ± 0.009
ASTER-01 (0.52–0.60)	0.187 ± 0.004	0.180 ± 0.006	B17 (0.89–0.92)	0.243 ± 0.005	0.235 ± 0.009
ASTER-02 (0.63–0.69)	0.232 ± 0.005	0.221 ± 0.008	B18 (0.93–0.94)	0.244 ± 0.006	0.237 ± 0.009
ASTER-03N (0.76–0.86)	0.250 ± 0.005	0.239 ± 0.009	B19 (0.92–0.97)	0.245 ± 0.006	0.237 ± 0.009
NAOMI-01 (0.46–0.52)	0.157 ± 0.003	0.151 ± 0.005			
NAOMI-02 (0.53–0.59)	0.188 ± 0.004	0.180 ± 0.006			
NAOMI-03 (0.63–0.70)	0.232 ± 0.005	0.221 ± 0.008			
NAOMI-04 (0.76–0.88)	0.249 ± 0.005	0.239 ± 0.009			
NAOMI-PAN (0.46–0.74)	0.203 ± 0.004	0.194 ± 0.007			

research concerning surface characterization. The possible differences in the ASTER GED bands need to be addressed in future research accounting for different soil sample collection, since one spectra can be used to characterize the site, but other spectra are required to estimate the possible variations of the soil in the same study area.

Figure 6 shows the in-situ and remote sensing LST for the ATAFIC study area. Also shown are the corresponding pixel footprints for each remote sensor and an in-situ LST time series between 30 min before and 30 min after the Landsat 8 overpass.

Table 4. Emissivities for the effective bandwidth of common sensors derived from measured emissivity spectra.

Sensor	Band	Bandwidth (μm)	E_f (μm)	Sand	Pebbles	Sand and pebbles
ETM+ (L7)	6	10.4–12.5	11.349	0.957	0.962	0.955
TIRS (L8)	10	10.60–11.19	10.904	0.951	0.958	0.947
	11	11.50–12.51	12.003	0.963	0.966	0.960
ASTER (TERRA)	10	8.125–8.475	8.287	0.947	0.956	0.947
	11	8.475–8.825	8.635	0.936	0.944	0.931
	12	8.925–9.275	9.079	0.93	0.931	0.921
	13	10.25–10.95	10.659	0.95	0.957	0.947
	14	10.95–11.65	11.289	0.951	0.957	0.948
MODIS (Terra)	20	3.66–3.84	3.788	0.652	0.824	0.719
	21	3.929–3.989	3.992	0.648	0.826	0.719
	22	3.929–3.989	3.972	0.648	0.826	0.719
	23	4.02–4.08	4.057	0.649	0.825	0.718
	24	4.433–4.498	4.473	0.73	0.865	0.779
	25	4.482–4.549	4.545	0.741	0.871	0.788
	27	6.535–6.895	6.771	0.956	0.964	0.957
	28	7.175–7.475	7.343	0.973	0.973	0.971
	29	8.4–8.7	8.529	0.939	0.947	0.935
	30	9.58–9.88	9.734	0.937	0.945	0.935
	31	10.78–11.28	11.019	0.951	0.957	0.947
	32	11.77–12.27	12.033	0.963	0.967	0.96
	33	13.185–13.485	13.365	0.972	0.974	0.97
	34	13.485–13.785	13.683	0.974	0.976	0.973
	35	13.785–14.085	13.913	0.974	0.975	0.974
	36	14.085–14.385	14.196	0.976	0.975	0.973

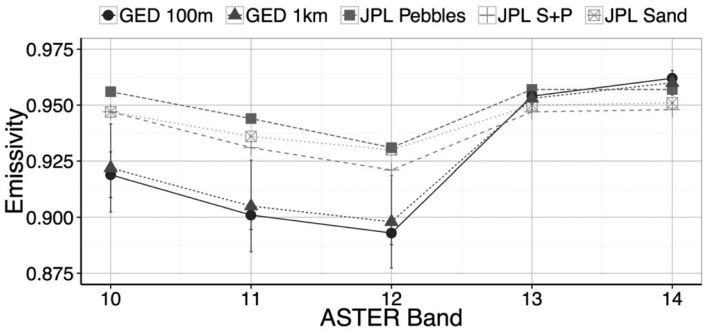

Figure 5. Emissivity values obtained from the laboratory spectra and the GED values for the 100 m pixel closest to the soil sample's collection site.

The area covered by a GOES pixel has an LST range of around 5 K, whereas the temperature range of a MODIS pixel is lower than 3 K, and less than 1 K for the area represented by the selected TIRS pixel. The in-situ LST evidenced a high surface thermal inertia, showing an increase from 304 to 316 K between 13:59 and 15:30 UTC for 21 August. A similar behavior was observed during 20 and 22 August . This temperature effect, in addition to the salt concentration (i.e. compounds derived from Na), affects the soil water availability (Kampf et al. 2005) and therefore limits the growth of vegetation cover, keeping the surface barren during the whole year. Nevertheless, the in-situ LST showed values similar to GOES, MODIS (Terra and Aqua) and TIRS (L8) LST at day and night times during the field campaign.

Despite the fact that ATAFIC study area is spatially homogenous, the changes in LST at the time of the L8 overpass (14:30 UTC; 11:30 local time) only allowed a short time period for acquiring in-situ measurements suitable to be compared to satellite retrievals. The small difference between Landsat and in-situ LST (<2 K) during the day allows considering this site for further works related to calibration or validation activities and in such case, in-situ data might be complemented by using more soil collection points for emissivity retrievals in order to decrease possible uncertainties. Despite the good agreement between in-situ and remote sensing LST during ATAFIC campaign, it is necessary to analyze the temporal variability of the LST in the past decade in order to evaluate the capabilities of the study area to be used as a possible site to validate LST retrieved from remote sensors. To this end, Figure 7 shows the long-term LST for the ATAFIC site derived from MODIS (Terra and Aqua) and its standard deviation.

At daytime, it can be seen that LST presents high annual amplitude (~20 K) where the annual mean standard deviation of LST derived from the Terra and Aqua is close to 4 K. The LST obtained at daytime shows higher values from Aqua than Terra; being consistent with the overpass times and presenting a higher variability during September to November. In contrast, the LST derived from Terra at daytime presents a lower variability than Aqua. For nighttime, both LST sources (Aqua and Terra) are quite similar during the year and the annual mean standard deviation of LST is lower than 2 K estimating a maximum and minimum variability of LST during July and December, respectively. There is important to mention that radiance-based method to estimate LST can be used for this site based on the homogeneous of ATAFIC and the emissivity spectra presented in this manuscript (Wan and Li 2008; Hulley and Hook 2012).

6. Discussion

Several requirements need to be fulfilled in order to consider the acquisition of surface parameters for spectroscopy and remote sensing applications (Milton, Fox, and Schaepman 2006). During ATAFIC, most of the activities for both the surface and atmospheric characterizations were performed applying pre-established in-situ measurement protocols in addition to laboratory measurements. The results presented here have demonstrated the advantages and usefulness of this area for the

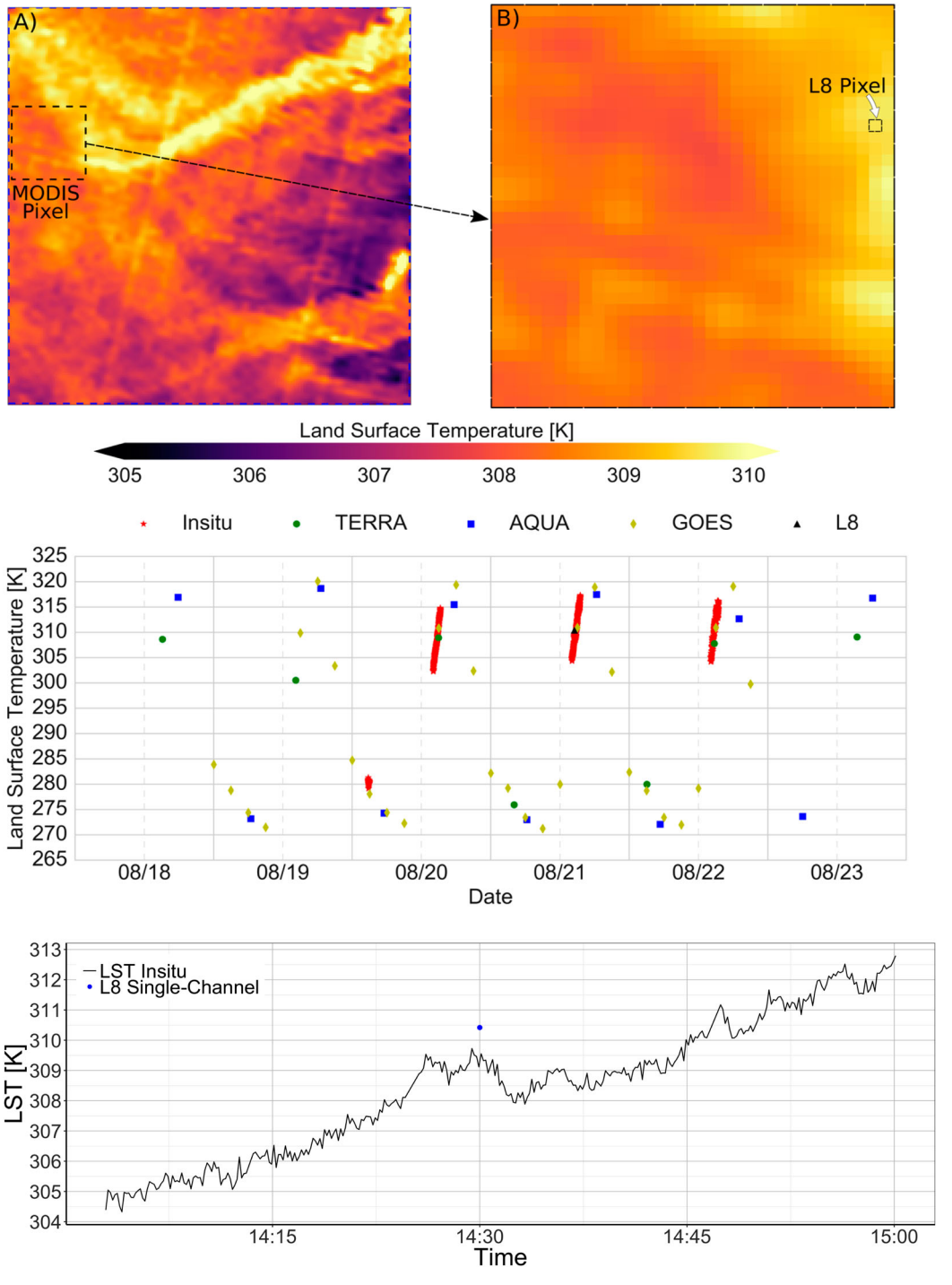

Figure 6. Top: (A) GOES pixel footprint (~5000 m^2) over the LST image retrieved from TIRS data using a Split-Window method over the ATAFIC field campaign area at 14:30 UTC 08/21 (with the location of the corresponding MODIS pixel), and (B) MODIS pixel footprint (~1000 m^2) showing the location of the L8 pixel (~30 m^2) corresponding to the selected site of in-situ measurements. Middle: LST values from in-situ measurements and retrieved by GOES, MODIS (Terra and Aqua) and TIRS (L8) over the ATAFIC campaign period. Bottom: In-situ and TIRS (SC and SW) LST for the ATAFIC study area at the time of the L8 overpass. Time is in UTC (Local time = UTC-3).

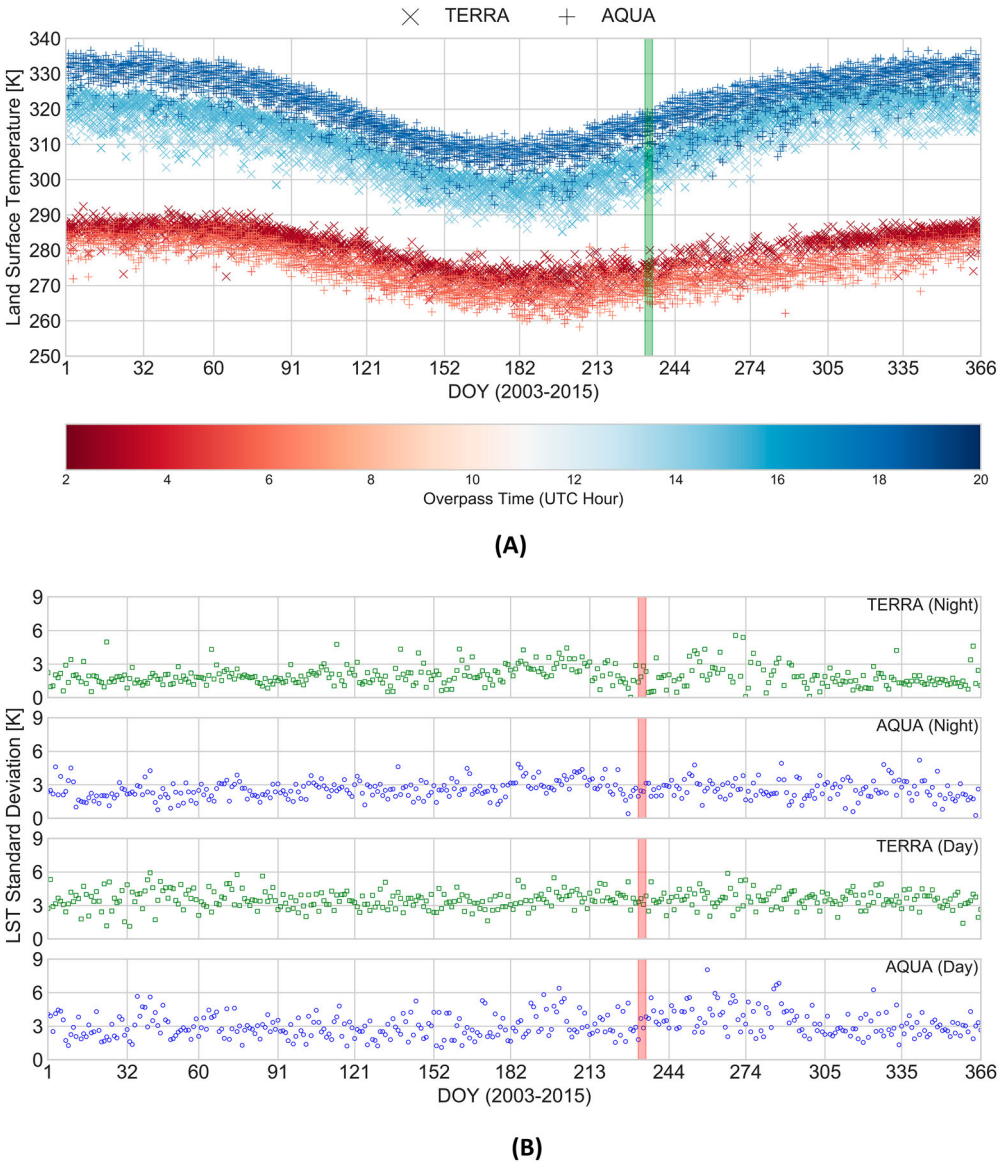

Figure 7. (A) Daily LST values from Terra and Aqua for the 2003–2015 period and its standard deviation (B) for the ATAFIC study area. The green rectangle shows the field campaign period.

acquisition of different types of data and for the execution of all mandatory activities that vicarious calibration and validation processes require, either for low, middle or high spatial resolution sensors. Moreover, the retrievals obtained from atmospheric measurements (Pinto et al. 2015) show that aerosol loading and water vapor content over this area are very low (i.e. less than 0.5 g cm^{-2}). The low water vapor concentration near the ATAFIC study area has been previously shown by Galewsky et al. (2011) and Cordero et al. (2016), who reported the lowest concentration of atmospheric water vapor in the surface of the Earth. Another important benefit of the Atacama desert is it's high frequency of clear-sky days, which was studied by Kiemle et al. (2015) with data from the Cloud-Aerosol Lidar and Infrared Pathfinder Satellite Observations (CALIPSO) level-2product. These atmospheric features also conditioned the Atacama Desert to be a target zone for testing

land surface emissivity/reflectance or atmospheric data bases derived from reanalysis (Jiménez-Muñoz et al. 2010; Mattar et al. 2015). MODTRAN 4.0 (Berk et al. 1998) simulations derived from ERA-Interim atmospheric profiles demonstrate the high values of atmospheric transmissivity during June, July and August for MODIS and Landsat thermal bands (Figure 8). In average, the atmospheric transmissivity is over 85% and decrease during the summer season (December, January and February) due to an increase in the water vapor content related to the Bolivian winter.

The surface emissivity spectra obtained for the soil sample collected at the study area showed a good agreement when compared to remote sensing data. The contrast between emissivity spectra and the ASTER GED showed the lowest bias for bands 13 and 14. As for bands 10, 11 and 12, the higher bias could be explained by the greater spatial and temporal heterogeneity of emissivity in these bands, and the fact that only one soil sample was used to obtain the laboratory emissivity spectra. Also, the ASTER calibration curve may not accurately represent the spectral variability in these types of soils. In the case of surface reflectance, radiometric measurements showed stable values for different measurement protocols applied in the study area. Despite these good results, further research needs to be addressed in order to evaluate the study area in terms of the spatial/temporal pseudo-invariance of the spectral behavior of the site or to perform vicarious calibration for optical remote sensing.

The long-term LST data derived from MODIS for the ATAFIC location showed low standard deviation ~2 K during nighttime and reasonable values at daytime demonstrated by in-situ data. The ATAFIC site presents a homogeneous land cover during the whole year that is not affected by local rainfall events often occurring during the austral summer, the so-called Invierno Boliviano. Similar works related to the validation of LST in desert areas evidence some green up during short periods of rainfall which generate changes in the land surface cover and therefore in the emissivity affecting the LST validation products (Göttsche et al. 2016), nevertheless this is not the case for the ATAFIC study area.

The efforts dedicated during ATAFIC can be considered as a milestone in South American remote sensing experiences, where new satellites administrated by locally space agencies or institutions of developing countries are becoming crucial for EO. For instance, the cases of the Brazilian program with forthcoming CBERS missions (Ponzoni and Albuquerque 2008) or the Fasat-Charlie (Mattar et al. 2014; Barrientos et al. 2016), which is the first successful Chilean satellite mission that can be calibrated or inter-compared with data from similar remote sensing sensors. In this particular case, the Atacama Desert could be used as a reference site for updating or validating current absolute calibration coefficients or for future vicarious calibration activities.

7. Conclusion

This manuscript describes and presents the first remote sensing field campaign carried out in the Atacama Desert. Surface and atmospheric measurements accompanied with laboratory analysis, showed that the study area has a high potential for further remote sensing applications. The extremely low atmospheric water vapor loading and the cloudiness patterns highlight the atmospheric conditions of the 'El Tambillo' zone. For LST and emissivity, the data collected during ATAFIC 2014 can be used for the preliminary test, although further works must be focused on the spatial heterogeneity of thermal remote sensing sensors such as MODIS or GOES. For the case of ASTER, Landsat or Sentinel-3 spatial resolution at the 100 m level, a low spatial variability has been estimated over the study area for thermal calibration or validation activities. Finally, the results showed in this work contribute to the definition of a potential site to develop calibration and validation protocols in South-America, the fact that will benefit current and forthcoming space missions. Indeed, ATAFIC 2014 is the first approach to consider the Atacama Desert in further calibration and validation remote sensing field campaigns.

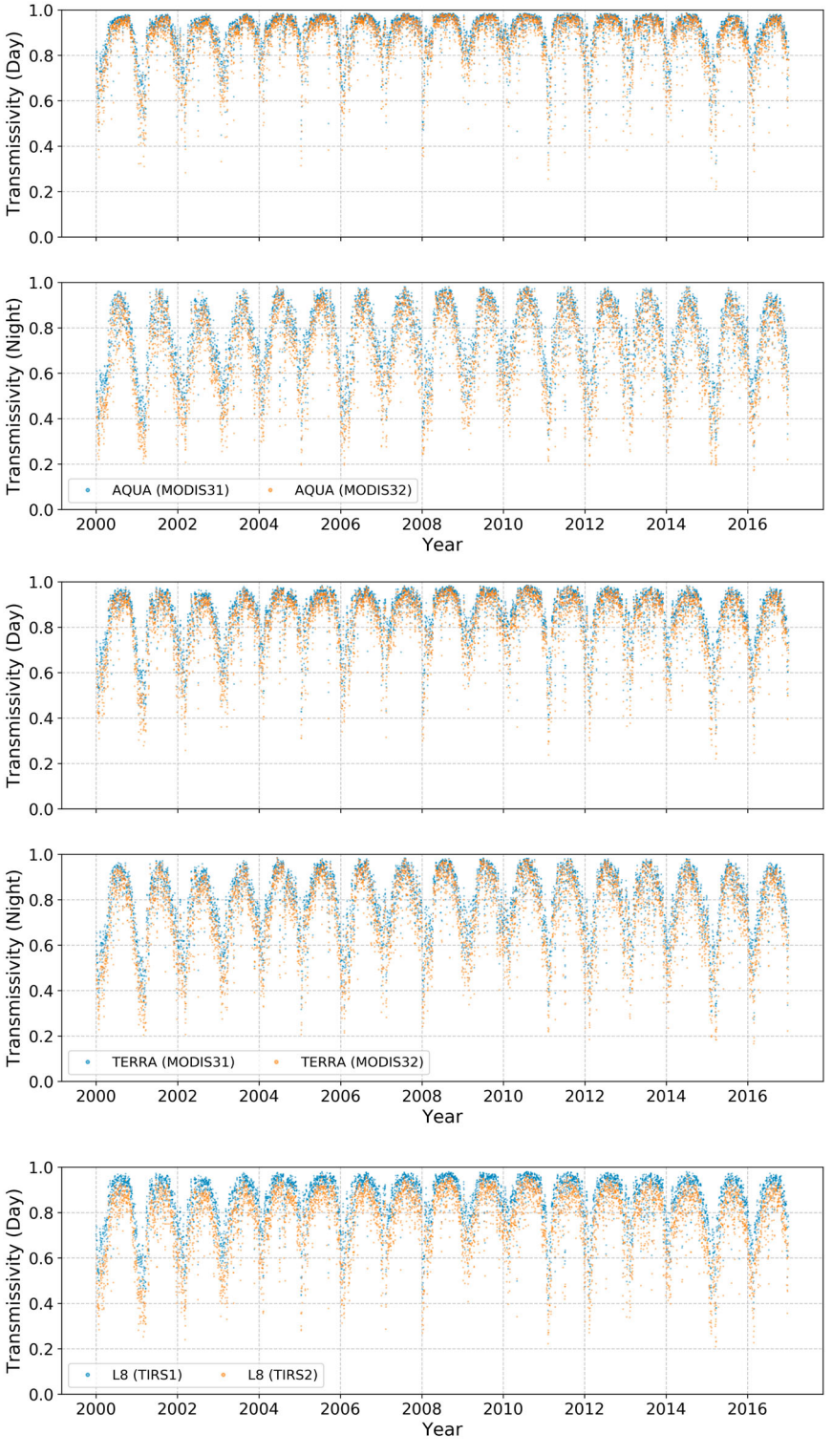

Figure 8. Atmospheric transmissivity for MODIS-AQUA (up), TERRA (medium) at day and night in addition to Landsat (bottom) for the time series for MOD07 product.

Acknowledgments

The authors would like to thank to Dr Juan Carlos Jimenez-Muñoz for his valuable comments and Dr Jaime Hernández for lending the ASD HandHeld field spectroradiometer.

Disclosure statement

No potential conflict of interest was reported by the authors.

Funding

This work was partially funded by Fondecyt Initial [CONICYT/ref-11130359]. The authors would also like to thank CNPq and CAPES for the scholarship given to Ms. Cibele T. Pinto and its research financial support.

ORCID

Cibele T. Pinto http://orcid.org/0000-0002-2895-8697

References

Azua-Bustos, Armando, Catalina Urrejola, and Rafael Vicuña. 2012. "Life at the Dry Edge: Microorganisms of the Atacama Desert." *FEBS Letters* 586 (18): 2939–2945. doi:10.1016/j.febslet.2012.07.025.

Baldridge, A. M., S. J. Hook, C. I. Grove, and G. Rivera. 2009. "The ASTER Spectral Library Version 2.0." *Remote Sensing of Environment* 113 (4): 711–715. doi:10.1016/j.rse.2008.11.007.

Barrientos, Carolina, Cristian Mattar, Theodoros Nakos, and Waldo Perez. 2016. "Radiometric Cross-calibration of the Chilean Satellite FASat-C Using RapidEye and EO-1 Hyperion Data and a Simultaneous Nadir Overpass Approach." *Remote Sensing* 8 (7): 612–610. doi:10.3390/rs8070612.

Berk, A., L. S. Bernstein, G. P. Anderson, P. K. Acharya, D. C. Robertson, J. H. Chetwynd, and S. M. Adler-Golden. 1988. "MODTRAN Cloud and Multiple Scattering Upgrades with Application to AVIRIS." *Remote Sensing of Environment* 65: 367–375. doi:10.1016/j.asr.2003.03.028.

Brown, Robert L., Wolfgang Wild, and Charles Cunningham. 2004. "ALMA – The Atacama Large Millimeter Array." *Advances in Space Research* 34 (3): 555–559. doi:10.1016/j.asr.2003.03.028.

Bullard, Joanna E., Kevin White, and Ian Livingstone. 2011. "Morphometric Analysis of Aeolian Bedforms in the Namib Sand Sea Using ASTER Data." *Earth Surface Processes and Landforms* 36 (11): 1534–1549. doi:10.1002/esp.2189.

Campbell, Petya K. Entcheva, Elizabeth M. Middleton, Kurt J. Thome, Raymond F. Kokaly, Karl Fred Huemmrich, David Lagomasino, Kimberly A. Novick, and Nathaniel A. Brunsell. 2013. "EO-1 Hyperion Reflectance Time Series at Calibration and Validation Sites: Stability and Sensitivity to Seasonal Dynamics." *IEEE Journal of Selected Topics in Applied Earth Observations and Remote Sensing* 6 (2): 276–290. doi:10.1109/JSTARS.2013.2246139.

Cereceda, P., H. Larrain, P. Osses, M. Farías, and I. Egaña. 2008. "The Spatial and Temporal Variability of Fog and Its Relation to Fog Oases in the Atacama Desert, Chile." *Atmospheric Research* 87 (3–4): 312–323. doi:10.1016/j.atmosres.2007.11.012.

Chander, Gyanesh, Tim J. Hewison, Nigel Fox, Xiangqian Wu, Xiaoxiong Xiong, and William J. Blackwell. 2013. "Overview of Intercalibration of Satellite Instruments." *IEEE Transactions on Geoscience and Remote Sensing* 51 (3): 1056–1080. doi:10.1109/TGRS.2012.2228654.

Chávez, R. O., Jan G P W Clevers, Martin Herold, Edmundo Acevedo, and Mauricio Ortiz. 2013. "Assessing Water Stress of Desert Tamarugo Trees Using in Situ Data and Very High Spatial Resolution Remote Sensing." *Remote Sensing* 5 (10): 5064–5088. doi:10.3390/rs5105064.

Chávez, R. O., J. G. P. W. Clevers, M. Herold, M. Ortiz, and E. Acevedo. 2012. "Modelling the Spectral Response of the Desert Tree Prosopis Tamarugo to Water Stress." *International Journal of Applied Earth Observation and Geoinformation* 21 (1): 53–65. doi:10.1016/j.jag.2012.08.013.

Clarke, Jonathan D. A. 2006. "Antiquity of Aridity in the Chilean Atacama Desert." *Geomorphology* 73 (1–2): 101–114. doi:10.1016/j.entcs.2005.12.035.

Cordero, R. R., A. Damiani, G. Seckmeyer, J. Jorquera, M. Caballero, P. Rowe, J. Ferrer, et al. 2016. "The Solar Spectrum in the Atacama Desert." *Scientific Reports* 6: 22457. doi:10.1038/srep22457.

Cosnefroy, Hélène, Marc Leroy, and Xavier Briottet. 1996. "Selection and Characterization of Saharan and Arabian Desert Sites for the Calibration of Optical Satellite Sensors." *Remote Sensing of Environment* 58 (1): 101–114. doi:10.1016/0034-4257(95)00211-1.

Durán-Alarcón, Claudio, Andrés Santamaría-Artigas, N. Valenzuela, and Cristian Mattar. 2014. "RSR Calculator, Una Herramienta Para El Proceso de Calibración/Validación." *Revista de Teledetección* 42: 111–117.

Fletcher, Lauren E., Julio E. Valdivia-Silva, Saul Perez-Montaño, Renee M. Condori-Apaza, Catharine A. Conley, and Christopher P. McKay. 2012. "Variability of Organic Material in Surface Horizons of the Hyper-arid Mars-like Soils of the Atacama Desert." *Advances in Space Research* 49 (2): 271–279. doi:10.1016/j.asr.2011.10.001.

Franch, B., E. F. Vermote, and M. Claverie. 2014. "Intercomparison of Landsat Albedo Retrieval Techniques and Evaluation Against In Situ Measurements Across the US SURFRAD Network." *Remote Sensing of Environment* 152: 627–637. doi:10.1016/j.rse.2014.07.019.

Freitas, Sandra C, Isabel F Trigo, João Macedo, Carla Barroso, Ricardo Silva, and Rui Perdigão. 2013. "Land Surface Temperature from Multiple Geostationary Satellites." *International Journal of Remote Sensing* 34 (9–10): 3051–3068. doi:10.1080/01431161.2012.716925.

Galewsky, Joseph, Christopher Rella, Zachary Sharp, Kimberly Samuels, and Dylan Ward. 2011. "Surface Measurements of Upper Tropospheric Water Vapor Isotopic Composition on the Chajnantor Plateau, Chile." *Geophysical Research Letters* 38 (17): 1–5. doi:10.1029/2011GL048557.

Garreaud, René D., Alejandra Molina, and Marcelo Farias. 2010. "Andean Uplift, Ocean Cooling and Atacama Hyperaridity: A Climate Modeling Perspective." *Earth and Planetary Science Letters* 292 (1–2): 39–50. doi:10.1016/j.epsl.2010.01.017.

Govaerts, Yves M., and Marco Clerici. 2004. "Evaluation of Radiative Transfer Simulations Over Bright Desert Calibration Sites." *IEEE Transactions on Geoscience and Remote Sensing* 42 (1): 176–187. doi:10.1109/TGRS.2003.815406.

Göttsche, Frank-M, and Glynn C. Hulley. 2012. "Validation of Six Satellite-retrieved Land Surface Emissivity Products Over Two Land Cover Types in a Hyper-arid Region." *Remote Sensing of Environment* 124: 149–158. doi:10.1016/j.rse.2012.05.010.

Göttsche, F.-M., F.-S. Olesen, and A. Bork-Unkelbach. 2013. "Validation of Land Surface Temperature Derived From MSG/SEVIRI with In Situ Measurements at Gobabeb, Namibia." *International Journal of Remote Sensing* 34 (9–10): 3069–3083. doi:10.1080/01431161.2012.716539.

Göttsche, Frank-M., Folke-S. Olesen, Isabel Trigo, Annika Bork-Unkelbach, and Maria Martin. 2016. "Long Term Validation of Land Surface Temperature Retrieved From MSG/SEVIRI with Continuous In-Situ Measurements in Africa." *Remote Sensing* 8 (5): 410. doi:10.3390/rs8050410.

Helder, Dennis, Kurtis J. Thome, Nischal Mishra, Gyanesh Chander, Xiaoxiong Xiong, Amit Angal, and Taeyoung Choi. 2013. "Absolute Radiometric Calibration of Landsat Using a Pseudo Invariant Calibration Site." *IEEE Transactions on Geoscience and Remote Sensing* 51 (3): 1360–1369. doi:10.1109/TGRS.2013.2243738.

Hubbard, Bernard E., and James K. Crowley. 2005. "Mineral Mapping on the Chilean-Bolivian Altiplano Using Co-orbital ALI, ASTER and Hyperion Imagery: Data Dimensionality Issues and Solutions." *Remote Sensing of Environment* 99 (1–2): 173–186. doi:10.1016/j.rse.2005.04.027.

Hulley, G. C., and S. J. Hook. 2012. "A Radiance-based Method for Estimating Uncertainties in the Atmospheric Infrared Sounder (AIRS) Land Surface Temperature Product." *Journal of Geophysical Research-Atmospheres* 117. doi:10.1029/2012JD018102.

Hulley, G., S. J. Hook, E. Abbott, N. Malakar, T. Islam, and M. Abrams. 2015. "The ASTER Global Emissivity Dataset (ASTER GED): Mapping Earth's Emissivity at 100 Meter Spatial Scale." *Geophysical Research Letters* 42: 7966–7976. doi:10.1002/2015GL065564.

Hulley, Glynn C., Simon J. Hook, and Alice M. Baldridge. 2009. "Validation of the North American ASTER Land Surface Emissivity Database (NAALSED) Version 2.0 Using Pseudo-invariant Sand Dune Sites." *Remote Sensing of Environment* 113 (10): 2224–2233. doi:10.1016/j.rse.2009.06.005.

Insel, Nadja, Christopher J. Poulsen, and Todd A. Ehlers. 2010. "Influence of the Andes Mountains on South American Moisture Transport, Convection, and Precipitation." *Climate Dynamics* 35 (7): 1477–1492. doi:10.1007/s00382-009-0637-1.

Jiménez-Muñoz, J. C., José A Sobrino, Cristian Mattar, and Belen Franch. 2010. "Atmospheric Correction of Optical Imagery from MODIS and Reanalysis Atmospheric Products." *Remote Sensing of Environment* 114 (10): 2195–2210. doi:10.1016/j.rse.2010.04.022.

Jiménez-Muñoz, J. C., J. A. Sobrino, Cristian Mattar, Glynn Hulley, and Frank-M. Göttsche. 2013. "Temperature and Emissivity Separation from MSG/SEVIRI Data." *IEEE Transactions on Geoscience and Remote Sensing* 52 (9): 1–15. doi:10.1109/TGRS.2013.2293791.

Jiménez-Muñoz, J. C., José A Sobrino, Drazen Skokovic, Cristian Mattar, and Jordi Cristobal. 2014. "Land Surface Temperature Retrieval Methods from Landsat-8 Thermal Infrared Sensor Data." *IEEE Geoscience and Remote Sensing Letters* 11 (10): 1840–1843. doi:10.1109/LGRS.2014.2312032.

Jungers, Matthew C., Arjun M. Heimsath, Ronald Amundson, Greg Balco, David Shuster, and Guillermo Chong. 2013. "Active Erosion-deposition Cycles in the Hyperarid Atacama Desert of Northern Chile." *Earth and Planetary Science Letters* 371–372: 125–133. doi:10.1016/j.epsl.2013.04.005.

Kampf, Stephanie K., Scott W. Tyler, Cristián A. Ortiz, José F. Muñoz, and Paula L. Adkins. 2005. "Evaporation and Land Surface Energy Budget at the Salar de Atacama, Northern Chile." *Journal of Hydrology* 310 (1–4): 236–252. doi:10.1016/j.jhydrol.2005.01.005.

Kiemle, C., G. Ehret, S. R. Kawa, and E. V. Browell. 2015. "The Global Distribution of Cloud Gaps in CALIPSO Data." *Journal of Quantitative Spectroscopy and Radiative Transfer* 153: 95–101. doi:10.1016/j.jqsrt.2014.12.001.

Krishnan, Praveena, John Kochendorfer, Edward J. Dumas, Pierre C. Guillevic, C. Bruce Baker, Tilden P. Meyers, and Borja Martos. 2015. "Comparison of In-Situ, Aircraft, and Satellite Land Surface Temperature Measurements Over a NOAA Climate Reference Network Site." *Remote Sensing of Environment* 165: 249–264. doi:10.1016/j.rse.2015.05.011.

Lacherade, Sophie, Bertrand Fougnie, Patrice Henry, and Philippe Gamet. 2013. "Cross Calibration Over Desert Sites: Description, Methodology, and Operational Implementation." *IEEE Transactions on Geoscience and Remote Sensing* 51 (3): 1098–1113. doi:10.1109/TGRS.2012.2227061.

Lester, Elizabeth D., Masataka Satomi, and Adrian Ponce. 2007. "Microflora of Extreme Arid Atacama Desert Soils." *Soil Biology and Biochemistry* 39 (2): 704–708. doi:10.1016/j.soilbio.2006.09.020.

Mattar, Cristian, C. Durán-Alarcón, Juan C. Jiménez-Muñoz, A. Santamaría-Artigas, L. Olivera-Guerra, and José A. Sobrino. 2015. "Global Atmospheric Profiles from Reanalysis Information (GAPRI): A New Database for Earth Surface Temperature Retrieval." *International Journal of Remote Sensing* 1161: 1–16. doi:10.1080/01431161.2015.1054965.

Mattar, Cristian, J. Hernández, Andrés Santamaría-Artigas, C. Durán-Alarcón, L. Olivera-Guerra, M. Inzunza, D. Tanre, and E. Escobar-lavín. 2014. "A First In-flight Absolute Calibration of the Chilean Earth Observation Satellite." *ISPRS Journal of Photogrammetry and Remote Sensing* 92: 16–25. doi:10.1016/j.isprsjprs.2014.02.017.

Miesch, Christophe, François Cabot, Xavier Briottet, and Patrice Henry. 2003. "Assimilation Method to Derive Spectral Ground Reflectance of Desert Sites from Satellite Datasets." *Remote Sensing of Environment* 87 (2–3): 359–370. doi:10.1016/j.rse.2003.08.013.

Milton, Edward J., Nigel P. Fox, and Michael E. Schaepman. 2006. "Progress in Field Spectroscopy." *International Geoscience and Remote Sensing Symposium (IGARSS)* 113: 1966–1968. doi:10.1109/IGARSS.2006.509.

Moreira-Munoz, Andres. 2011. *Plant Geography of Chile. Vol. 5. Plant and Vegetation*. Dordrecht: Springer. doi:10.1007/978-90-481-8748-5.

Morgan, A. M., A. D. Howard, D. E. J. Hobley, J. M. Moore, W. E. Dietrich, R. M. E. Williams, D. M. Burr, J. A. Grant, S. A. Wilson, and Y. Matsubara. 2014. "Sedimentology and Climatic Environment of Alluvial Fans in the Martian Saheki Crater and a Comparison with Terrestrial Fans in the Atacama Desert." *Icarus* 229: 131–156. doi:10.1016/j.icarus.2013.11.007.

Muñoz, C., N. Guerra, J. Martínez-Frías, R. Lunar, and J. Cerda. 2007. "The Atacama Desert: A Preferential Arid Region for the Recovery of Meteorites-find Location Features and Strewnfield Distribution Patterns." *Journal of Arid Environments* 71 (2): 188–200. doi:10.1016/j.jaridenv.2007.03.007.

Nagaraja Rao, C. R., J. Chen, J. T. Sullivan, and N. Zhang. 1999. "Calibration of Meteorological Satellite Sensors." *Advances in Space Research* 23 (8): 1357–1365. doi:10.1016/0273-1177(95)00439-L.

Olesen, Folke-S., and Frank-M. Göttsche. 2009. "Validation of Land Surface Temperatures Obtained from METEOSAT-MVIRI and SEVIRI with In-Situ Measurements." 2009 EUMETSAT meteorological satellite conference, Bath, September 21–25, No. Figure 1.

Pinto, Cibele T., Flavio J. Ponzoni, C. Barrientos, Cristian Mattar, Andrés Santamaría-Artigas, and Ruy M. Castro. 2015. "Spectral and Atmospheric Characterization of a Site at Atacama Desert for Earth Observation Sensor Calibration." *IEEE Geoscience and Remote Sensing Letters* 12 (11): 2227–2231. doi:10.1109/LGRS.2015.2460454.

Ponzoni, Flávio Jorge, and Bráulio Fonseca Carneiro Albuquerque. 2008. "Pre-launch Absolute Calibration of CCD/CBERS-2B Sensor." *Sensors* 8 (10): 6557–6565. doi:10.3390/s8106557.

Ramachandran, Bhaskar, Christopher O. Justice, and Michael J. Abrams. 2011. Land Remote Sensing and Global Environmental Change. In *Remote Sensing and Digital Image Processing*, edited by Bhaskar Ramachandran, Christopher O. Justice, and Michael J. Abrams. New York: Springer. doi:10.1007/978-1-4419-6749-7.

Richards, J. P., A. J. Boyce, and M. S. Pringle. 2001. "Geologic Evolution of the Escondida Area, Northern Chile: A Model for Spatial and Temporal Localization of Porphyry Cu Mineralization." *Economic Geology* 96 (2): 271–305. doi:10.2113/gsecongeo.96.2.271.

Rodwell, M. J., and B. J. Hoskins. 2001. "Subtropical Anticyclones and Summer Monsoons." *Journal of Climate* 14 (15): 3192–3211. doi:10.1175/1520-0442(2001)014<3192:SAASM>2.0.CO;2.

Rutllant, José A., Humberto Fuenzalida, and Patricio Aceituno. 2003. "Climate Dynamics Along the Arid Northern Coast of Chile: The 1997–1998 Dinámica Del Clima de La Región de Antofagasta (DICLIMA) Experiment." *Journal of Geophysical Research* 108 (D17): 1–13. doi:10.1029/2002JD003357.

Salisbury, J. W., and D. M. D'Aria. 1992. "Emissivity of Terrestrial Materials in the 8-14μm Atmospheric Window." *Remote Sensing of Environment* 42: 83–106.

Salisbury, John W., Andrew Wald, and Dana M. D'Aria. 1994. "Thermal-infrared Remote Sensing and Kirchhoff's Law. 1: Laboratory Measurements." *Journal of Geophysical Research* 99: 11897–11911. doi:10.1029/93JB03600.

Scott, Karen P., Kurtis J. Thome, and Michelle R. Brownlee. 1996. "Evaluation of Railroad Valley Playa for Use in Vicarious Calibration." In *Proc. SPIE. International Society for Optics and Photonics*, edited by Brian Huberty, Joan B. Lurie, Jule A. Caylor, Pol Coppin, and Pierre C. Robert. doi:10.1117/12.256090.

Servicio Nacional de Geología y Minería de Chile (Sernageomin). 2003. *Mapa Geologico de Chile: Version Digital*, 25. Publicacion Geologia Digital 4.

Sobrino, J. A., B. Franch, C. Mattar, J. C. Jiménez-Muñoz, and C. Corbari. 2012. "A Method to Estimate Soil Moisture from Airborne Hyperspectral Scanner (AHS) and ASTER Data: Application to SEN2FLEX and SEN3EXP Campaigns." *Remote Sensing of Environment* 117: 415–428. doi:10.1016/j.rse.2011.10.018.

Sobrino, J. A., J. C. Jiménez-Muñoz, G. Sòria, M. Gómez, A. Barella Ortiz, M. Romaguera, M. Zaragoza, et al. 2008. "Thermal Remote Sensing in the Framework of the SEN2FLEX Project: Field Measurements, Airborne Data and Applications." *International Journal of Remote Sensing* 29 (17–18): 4961–4991. doi:10.1080/01431160802036516.

Sobrino, J. A., C. Mattar, J. P. Gastellu-Etchegorry, J. C. Jiménez-Muñoz, and E. Grau. 2011. "Evaluation of the DART 3D Model in the Thermal Domain Using Satellite/Airborne Imagery and Ground-based Measurements." *International Journal of Remote Sensing* 32: 7453–7477. doi:10.1080/01431161.2010.524672.

Sobrino, J. A., C. Mattar, P. Pardo, J. C. Jiménez-Muñoz, S. J. Hook, A. Baldridge, and R. Ibañez. 2009. "Soil Emissivity and Reflectance Spectra Measurements." *Applied Optics* 48: 3664–3670. doi:10.1364/AO.48.003664.

Takahashi, Ken, and David S. Battisti. 2007. "Processes Controlling the Mean Tropical Pacific Precipitation Pattern. Part I: The Andes and the Eastern Pacific ITCZ." *Journal of Climate* 20 (14): 3434–3451. doi:10.1175/JCLI4198.1.

Wan, Zhengming. 1999. "MODIS Land-surface Temperature Algorithm Theoretical Basis Document (LST ATBD)." https://modis.gsfc.nasa.gov/data/atbd/atbd_mod11.pdf.

Wan, Z., and Z. L. Li. 2008. "Radiance-based Validation of the V5 MODIS Land-surface Temperature Product." *International Journal of Remote Sensing* 29: 5373–5395.

Wang, Fan, Greg Michalski, Ji hye Seo, and Wensheng Ge. 2014. "Geochemical, Isotopic, and Mineralogical Constraints on Atmospheric Deposition in the Hyper-arid Atacama Desert, Chile." *Geochimica et Cosmochimica Acta* 135: 29–48. doi:10.1016/j.gca.2014.03.017.

Wettergreen, David, Deepak Bapna, Mark Maimone, and Geb Thomas. 1999. "Developing Nomad for Robotic Exploration of the Atacama Desert." *Robotics and Autonomous Systems* 26 (2–3): 127–148. doi:10.1016/S0921-8890(99)80002-5.